pH Stimuli Responsive Dextran Gated Mesoporous Silica as a Viable Delivery Vehicle

Yusuf Olatunji WAIDI[1]

1. Materials Science and Engineering Department, African University of Science and Technology, Abuja, Nigeria

Abstract

Mesoporous materials hold immense potential due to their diverse applications (catalysis, separation, drug delivery, etc.) viability. To unlock this potential, controlling the transport of molecules within their nanochannels is crucial. This study explores a novel technique to manipulate pore properties by hetero-functionalizing mesoporous silica with carboxylic acid and propylamine groups, creating pH-responsive surfaces. The negatively charged surface at basic pH attracts and loads a cationic dye through electrostatic interactions. This cargo can be efficiently released by switching to acidic pH, reversing the surface charge. Furthermore, the system incorporates dextran as a "gatekeeper" for controlled release. The study demonstrates significant differences in release profiles between functionalized materials, highlighting the effectiveness of this approach. Notably, the functionalization method strategy using 1,4-dioxane and appropriate reaction timing enables the desired properties for the first time. This work paves the way for designing advanced mesoporous materials with tailored functionalities for various applications.

Keywords: Mesoporous Silica, pH-responsive, Functionalizations, Delivery System

Graphical Abstract

1. Introduction

The field of nanomedicine, utilizing nanoparticles for medical intervention, has captivated chemists and chemists alike over the past decades.[1-4] Mesoporous silica nanoparticles (MSNs) have thrived into a leading contender in nanomedicine since their initial synthesis in the 1990s.[5-7] This potential was further solidified in 2001 by Vallet-Regi et al.'s groundbreaking demonstration of their application in drug delivery.[8] These nanoparticles possess unique properties, including a confined space ideal for encapsulating therapeutic compounds, which has spurred numerous research groups to develop MSN-based drug delivery systems.[9-11] MSNs own exceptional properties like high surface area, finely tunable pore structures, and abundant silanol groups, enabling versatile functionalization inside and out.[12-14] The breakthrough discovery of gated MSNs in the 2000s, particularly those functional in water, opened doors for developing sophisticated materials with stimuli-responsive molecular gates.[15, 16] Attached to

the MSN surface, these gatekeepers act as nano valves, blocking cargo release until triggered by a specific chemical, biochemical, or physical stimulus, often cleaving the gate and unleashing the cargo.[17, 18] This precise control over cargo release empowers MSNs to function as efficient drug delivery systems, enhancing biocompatibility, cellular uptake, controlled release of drugs, targeted delivery, and therapeutic molecules.[19-22]

Gated MSNs have emerged as versatile tools with diverse biomedical applications beyond drug delivery. They can encapsulate and deliver various therapeutic agents like proteins, drugs, or genes for bioimaging and treatment modalities like radiotherapy, photothermal therapy, and tissue engineering.[23, 24] Their gated nature allows for controlled release triggered by specific stimuli, minimizing premature leakage and unwanted side effects.[25-30] Additionally, gated MSNs extend beyond medicine, finding applications in sensing and communication due to their unique properties.[31-34] Due to their unique chemical properties, nanomaterials offer the potential to be designed for various applications. This has created numerous MSNs with diverse compositions, structures, and functionalities. These MSNs have shown promising cytotoxicity, therapeutic efficacy, and biocompatibility results. For comprehensive details on the Synthesis of MSNs, refer to the extensive review by Croissant et al.[35]

Unlike unmodified materials that suffer from premature drug release [36-40], surface-modified silica nanocarriers offer significant protection, enabling controlled delivery via various stimuli like pH, temperature, enzymes, and magnetic fields. The differing pH ranges across tissues and organs make pH-responsive systems particularly effective.[41-43] The weakly acidic environment found in many tissues serves as an ideal trigger for targeted drug release [44], highlighting the potential of pH-responsive MSN for numerous biomedical needs, including anticancer therapy [45, 46], gastrointestinal and ocular drug delivery and even gene therapy. This approach ensures the drugs

reach their intended destination and release their therapeutic effect at the precise time and location, maximizing their efficacy while minimizing potential side effects.

In this report, we designed a system to release cargo from MSN using dextran as a gatekeeper. The engineered silica has a pH-dependent surface charge, allowing cargo to be loaded at high pH and released at lower pH. However, previous designs only worked at very low pH (3), making them unsuitable for applications like cancer therapy. Therefore, we addressed this using a combination of carboxylic acid and propylamine groups, switching charges at a more relevant pH. Dextran was then attached to block the pores at high pH, preventing cargo release. Finally, lowering the pH triggered dextran detachment and cargo release, demonstrating a promising system for controlled cargo delivery.

2. Materials and Experiment

2.1 Materials.

We utilized various chemicals, including tetraethoxysilane (TEOS), 1-ethyl-3-(3-(dimethylamino)propyl)carbodiimide hydrochloride (EDC), 3-(2-Aminoethylamino)propyl] trimethoxysilane (AEAPS), dextran (Mr 6000 and 100000), cetyltrimethylammonium bromide (CTAB), succinic anhydride, and N-hydroxysuccinimide (NHS). These chemicals were acquired from various suppliers, including Sigma-Aldrich (AEAPS, TEOS, dextran), TCI Chemicals (EDC), Alfa Aesar (CTAB), Fluka (NHS), and Merck (succinic anhydride). They were employed as received with no additional purification.
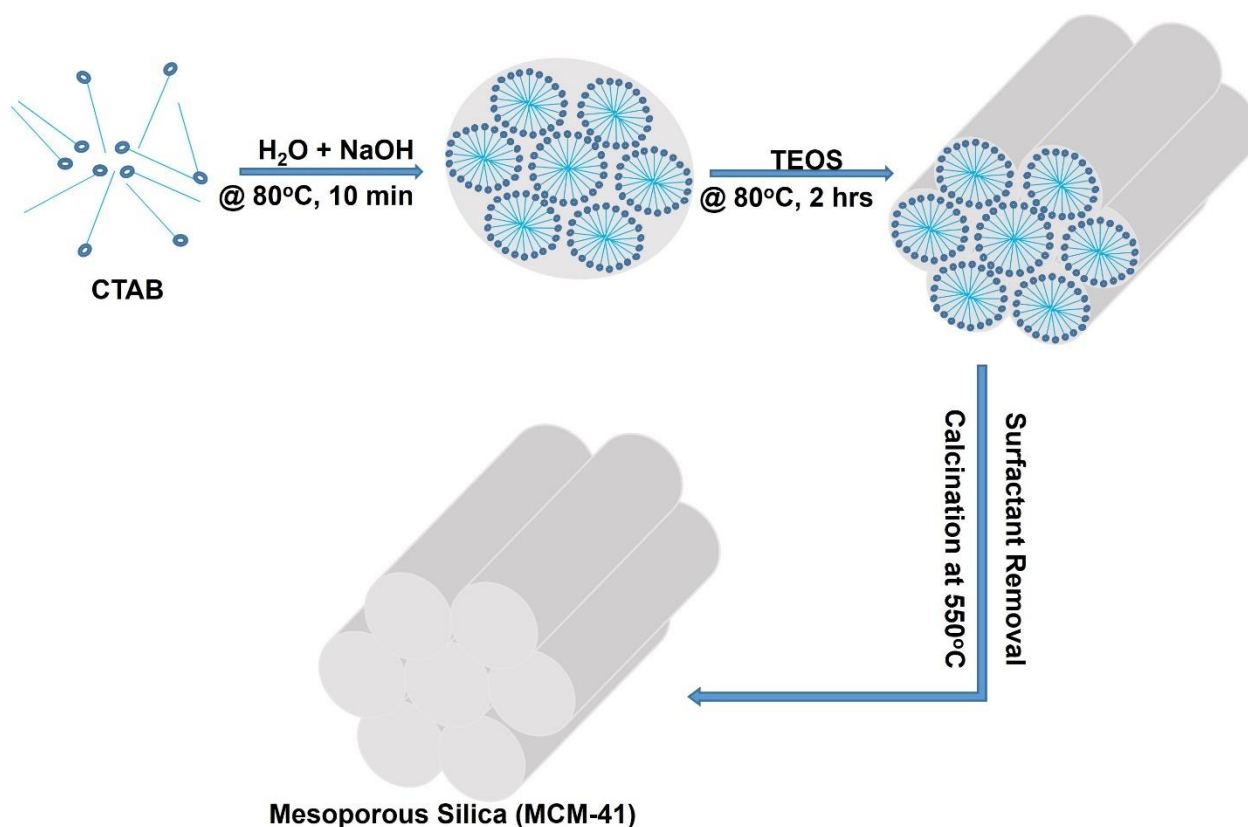
2.2 MCM-41 synthesis.

The reported synthesis of MCM-41 nanoparticles followed a previously established method.[47] Briefly, CTAB and NaOH were dissolved in water at elevated temperatures. TEOS was then slowly

added, allowing the reaction to proceed for 2 hours. The formed solid was isolated, washed, and dried. The nanoparticles were calcined to remove the templating agent.

2.3 MCM-N synthesis.

High vacuum-dried MCM-41 (1g) was added to anhydrous toluene (80 mL) and bath sonicated to form a homogeneous mixture. Then, APTES (1mL) was added to the mixture and refluxed under N_2 condition for 1 day with stirring. The mixture was centrifuged and thoroughly cleaned with toluene, hexane, and ethanol. Lastly, the product was vacuum-dried for 6 hours at 80 °C.

Scheme 1. Synthesis of MCM-41

2.4 MCM-Z synthesis.

MCM-N (0.5 g) was added to 1,4-dioxane (25 mL) and sonicated for a few minutes to create a homogeneous mixture. Subsequently, a solution of succinic anhydride (20 mg, 0.2 mmol) in 1,4-dioxane (12.5 mL) was added under stirring. The mixture was then heated for 10 minutes at 80 °C to facilitate the reaction. Finally, the product was isolated by centrifugation, cleaned with water and ethanol, and oven-dried overnight.
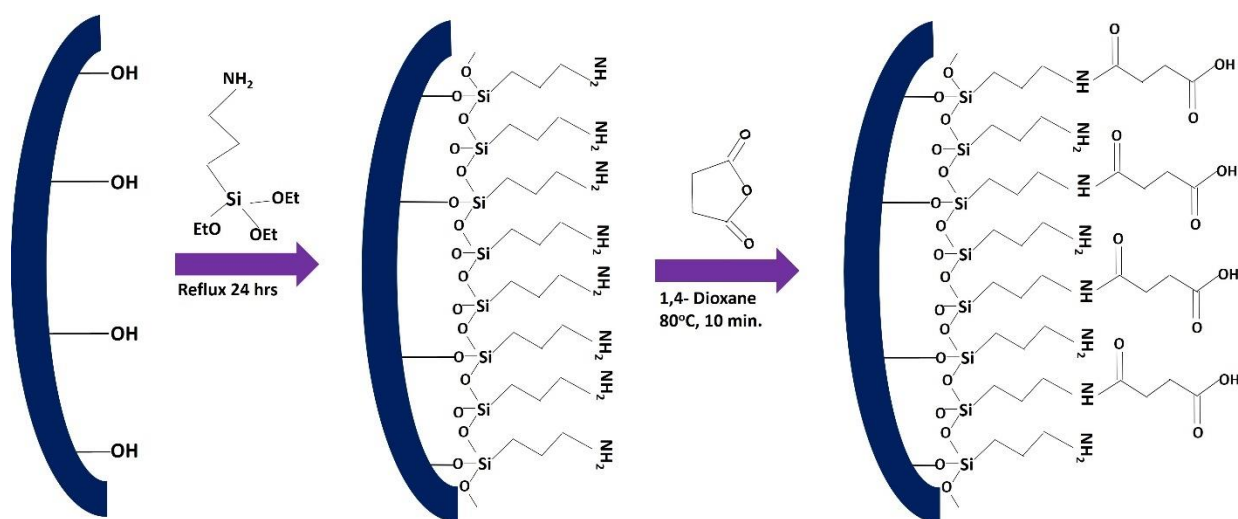
Scheme 2: Modifification of MCM-41 to obtain pH-responsive MCM-Z

2.5 Zeta potential.

MCM-41, MCM-N, and MCM-Z nanoparticles were dispersed in their respective buffers at 0.5 mg/mL concentrations. A Zetasizer Nano ZS instrument, manufactured by Malvern Instruments in the UK, was used to conduct the measurements. This instrument is equipped with a 532-nanometer laser and configured for a 173-degree backscattering angle. The temperature was maintained at 25°C using the instrument's built-in thermostat.

2.6 Preparation of samples for N₂ adsorption-desorption.

To thoroughly remove any adsorbed contaminants and prepare for gas adsorption analysis, the samples underwent a degassing pretreatment for 12 hours at 85 °C under a high vacuum. Subsequently, N_2 adsorption-desorption measurements were conducted at the cryogenic temperature of -196 °C

2.7 CV+ dye loading to MCM-Z.

Mesoporous channels of MCM-Z were efficiently loaded with CV+ using a simple two-step method. Firstly, MCM-Z (5 mg) was added to 1.95 mL of Tris buffer (pH 8.0, 10 mM). CV+ dye (0.05 mL, 0.5 mM) was dispersed, and the mixture was stirred for half a day at ambient conditions. The loaded MCM-Z was cleaned using Tris buffer to eliminate unbound molecules. Finally, the amount of loaded CV+ was quantified using UV-vis spectroscopy via a final and supernatant dispersion analysis.

2.8 MCM-Z Dextran capping (MCM-ZD).

In the first step, MCM-Z-loaded samples were thoroughly mixed in PBS at pH 7.4 to achieve a uniform mixture. Next, the particles were coated with dextran by adding dextran solution (4 mL, 25 mg/mL) and stirring the mixture for 3 hours to facilitate dextran-MCM-Z surface interaction. Subsequently, the coated particles were isolated and rinsed with PBS buffer to eliminate unbound dextran molecules. Finally, the CV+-loaded MCM-Z particles were re-suspended in an aqueous solution, preparing them for subsequent analysis.

2.9 CV+ pH-dependent release.

To investigate CV+ release from dextran-coated and uncoated nanoparticles at different temperatures and pH conditions. Each nanoparticle (5 mg) was gently dispersed in PBS (1 mL, 10 mM) buffer solution at specific pH values. Aliquots of 0.2 mL were extracted every hour at

various temperature conditions (room, 37°C, 41°C, and 47°C). The sample volume was maintained by adding PBS. The quantity of CV+ released was quantified using UV-visible absorbance. This experiment design allowed for the evaluation of CV+ release kinetics under various temperature and pH conditions.

2.10 General characterization and equipment.

The material's crystalline structure was examined by powder X-ray diffraction (XRD) with specific parameters (step size: 0.02°, λ = 1.54 Å, voltage: 40 kV, current: 30 mA) on a Bruker-D8 diffractometer. After proper sample preparation, nitrogen adsorption-desorption at -196 °C provided insights into its surface area using an Autosorb-1C instrument, with the BET method and Quantachrome software aiding in data analysis. High-purity gases were employed throughout the analysis. Thermal stability was assessed by Mettler Toledo 850 for thermogravimetric analysis (TGA) under an oxygen condition with a specific heating rate (30-1000°C, 10°C/min). Functional groups were identified through Fourier transform infrared (FT-IR) spectroscopy with a Bruker IFS 66v/S instrument. Zeta potential and pH value were also conducted to gain further insights into the material's surface properties.

3. Discussion of Results

3.1 Synthesis and functionalizations analysis.

MCM-41 was first synthesized using an established sol-gel method (Scheme 1). The surface of these spheres was then covalently modified with (3-aminopropyl)triethoxysilane, introducing amine groups and creating MCM-N (Scheme 2). To further functionalize the surface, some of these amine groups were subsequently reacted with succinic anhydride, transforming MCM-N into

MCM-Z. This final material has a zwitterionic character, meaning it has both positively charged amine and negatively charged carboxyl groups decorating its nanochannel surfaces.

3.2 Quantitative functionalization calculation.

MCM-N:

TGA was conducted to determine the amount of organic molecule coupling to MCM-41 to make MCM-N. The analysis revealed 19.4% of weight coupling.

Hence, the total propylamine group = 1.94 mmol/g

Therefore, from the number of molecules of a substance = amount of that substance x Avogadro's constant,

We have the number of propylamine molecules = 1.94 x Avogadro's constant

$$= 1.94 \text{ x } 6.02 \text{ x } 10^{23}$$

$$= 1.16788 \text{ x } 10^{24} \text{ molecules/g}$$

However, the MCM-41 surface area = 987 m^2/g

$$= 987 \text{ x } 10^{18} \text{ nm}^2\text{/g}$$

Number of propylamine groups per nm^2 = 1.16788 x 10^{24} molecules / 987 x 10^{18} nm^2

$$= \textbf{1183 molecules / nm}^2$$

MCM-Z:

TGA was conducted to determine the carboxylic group coupling to MCM-N to make MCM-Z. The analysis revealed 3 % of weight coupling.

Hence, the total carboxylic acid group = 0.3 mmol/g

Number of -COOH group = 0.3 mmol x 6.02 x 10^{23}

= 1.806x 10^{23} molecules/g

Number of carboxylic acid moieties per nm^2 = 1.806 x 10^{23} molecules / 987 x 10^{18} nm^2

= 182.97 molecules/ nm^2

3.3 Structural and functionalizations quantification analysis.

The hexagonal mesostructure of MCM, MCM-N, and MCM-Z was retained during functionalization, as evidenced by the XRD patterns of low peak angle at $2\theta \approx 2.2$ (Fig 1.a). The TEM morphology of the synthesized MCM-41 is shown in Fig. 1.c and 1.d. revealing a hexagonal mesostructured and particle sizes around 90nm. TGA revealed that the MCM-N propylamine coupling was significantly higher than the MCM-Z carboxylic acid groups at 1.94 mmol g-1 and 0.3 mmol g-1, respectively (Fig 1.b). This shows that roughly 14% of the amine groups in MCM-N were bonded covalently through an amide linkage to the -COOH, highlighting a desired functionalization process as opposed to the previous study where the carboxylic acid group linked to the amine group was 56% percent [48], thus making it more protonated and hence undesirable for molecule sustained release at pH 5.
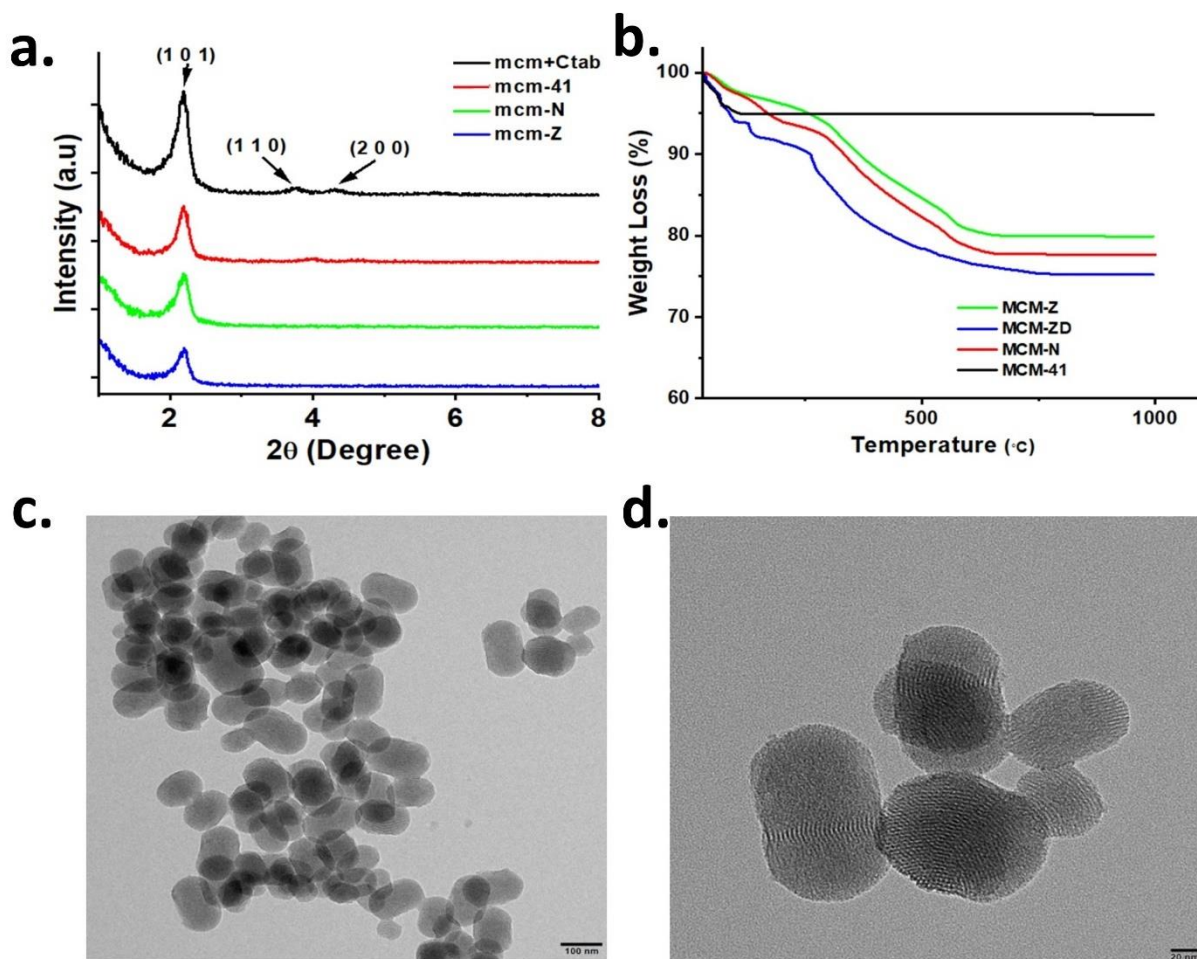
Fig.1. Showing the developed mesoporous nanoparticles structure and functionalizations quantifications. (a) XRD pattern (b) TGA (c) TEM at low mag. (d) TEM at high mag.

3.4 BET analysis.

The N_2 adsorption-desorption analysis, conducted at -196°C, confirmed progressive functionalization within the nanochannels of the materials (Fig. 2.a). The pore size distributions, determined using the Barrett-Joyner-Halenda (BJH) method, showcased a gradual decrease in average pore size from 2.5 nm for MCM to 2.1 nm for MCM-N and 1.9 nm for MCM-Z (Fig. 2.b). This trend implies continuous functionalization within the nanochannels. Further assessment using N_2 sorption and TGA studies estimated that the amount of propylamine in MCM-N was 1183

molecules per nm^2, while the quantity of carboxylic acid in MCM-Z was around 182.97 molecules per nm^2. These results collectively demonstrate the successful incorporation of functional groups within the nanochannels of the synthesized materials.

3.5 FTIR analysis.

Fig. 2.c displays the modified MSN and unmodified MSN FT-IR spectra. Notably, the unpurified MCM-41 exhibits characteristic peaks at 2924 cm^{-1}, 2854 cm^{-1} for C-H stretching, and 1491 cm^{-1} for C-H deformation, signifying the CTAB molecule's presence.[49] These peaks vanish in the purified sample, confirming the removal of CTAB (Fig. 2.c.). Furthermore, strong absorption bands at 1086.69 cm^{-1} and 962.3 cm^{-1} are observed for MCM-41, primarily attributed to Si-O-Si bridges' stretching and asymmetric stretching, and skeletal C-O bond vibrations, respectively, as documented in.[50] The characteristic peak confirmed the presence of NH$_2$ groups bound to the surface of MCM-41 at 1559.2 cm^{-1}, corresponding to the amide I stretching vibration and -NH$_2$ bending. Following the introduction of succinic anhydride, a new peak emerged at 1718 cm^{-1}, signifying the successful incorporation of carboxyl groups (derived from succinic anhydride) onto the surface, as evidenced by the carboxylic acid carbonyl stretch (C=O). Finally, the reduction in stretching observed at 3396 cm^{-1} indicated the presence of dextran molecules. Overall, the FT-IR analysis effectively verifies the presence and successful removal of CTAB and provides key structural information about the MCM-41 and the coupled materials.
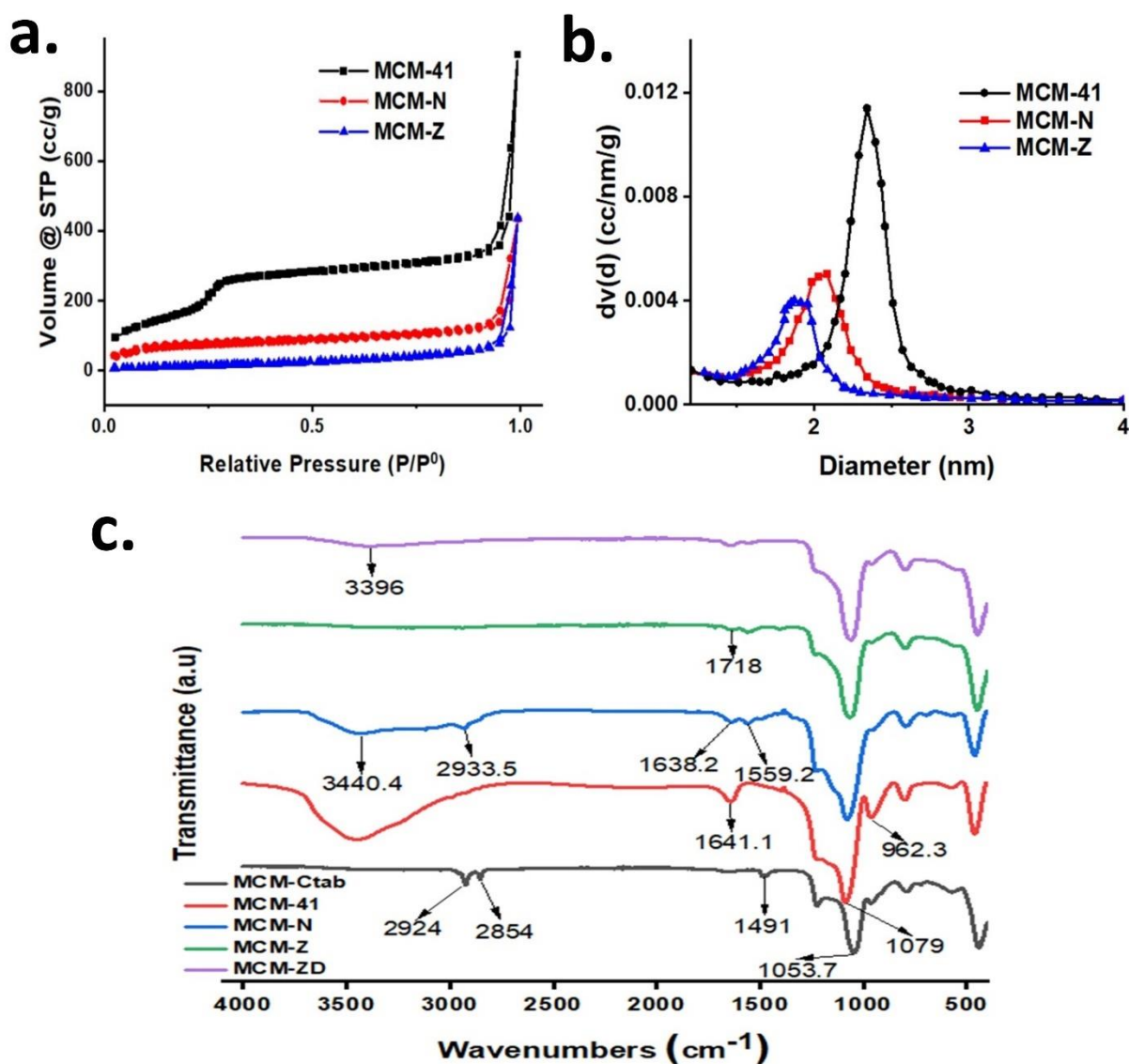
Fig 2. Showing the developed mesoporous nanoparticles pore volume and functionalizations group. (a) N_2 adsorption-desorption isotherm (b) Pore size distribution curves (c) FTIR.

3.6 ZETA potential.

The fabrication of MCM-Z was affirmed by zeta potential analysis, as illustrated in Fig 3. Initially, MCM-N exhibited a positive zeta potential of $+7.36 \pm 2$ mV at pH 7.4, indicating a positively charged surface (Fig 3 a.iii). However, the deprotonated carboxylic acid groups on the silica

nanochannels of MCM-Z resulted in a negative zeta potential of -11.5 ± 1 mV (Fig 3 b.iii), demonstrating a clear charge reversal. Further characterization at various pH values revealed that the protonation of amine groups on MCM-Z led to a positive zeta potential of +33.4 ± 1 mV around pH 5.0. These results offer clear evidence for the successful synthesis and distinct surface properties of MCM-Z. The zeta potential of MCM-ZD decreased with increasing pH, reaching a point of zero charge (PZC) of around 6.5. Further increase in pH caused a further reduced zeta potential at pH 7.5 to -24 ± 0.9 mV, likely due to carboxylate groups the formation. Zeta potential measurements at different pH values also characterized the charge reversal of MCM-ZD. The nanoparticle surface charge was positive at low pH due to amine group protonations (+21.5 mV zeta potential at pH 5.0). As the pH increased, the surface charge became neutral at the PZC of around 6.5. Further increase in pH caused a negative surface charge as a result of carboxylate group formation (-24 mV zeta potential at pH 7.5). Overall, Zeta potential measurements confirm the successful synthesis of MCM-Z, which exhibits unique surface properties due to the presence of both amine and carboxylic acid groups. Depending on pH, these groups cause reversible changes in surface charge, potentially impacting applications involving interactions with other molecules. It's vital to note that the specific values of zeta potential and point of zero charge may vary slightly depending on the exact synthesis conditions.
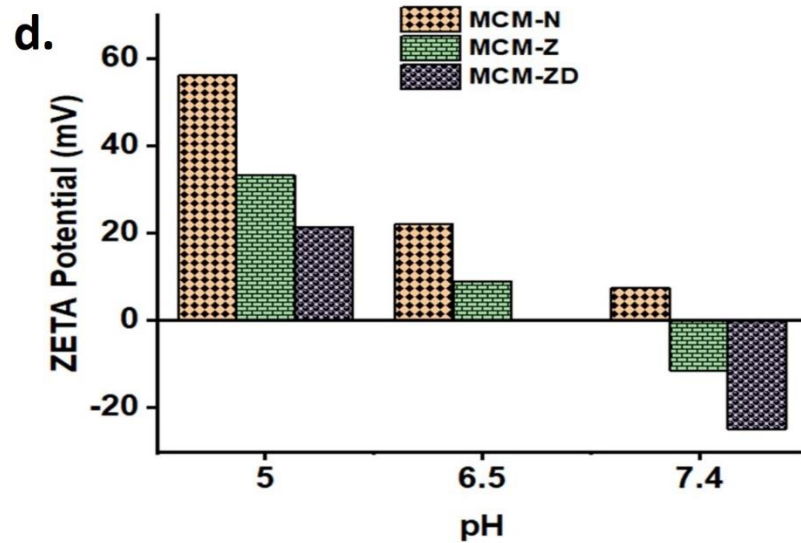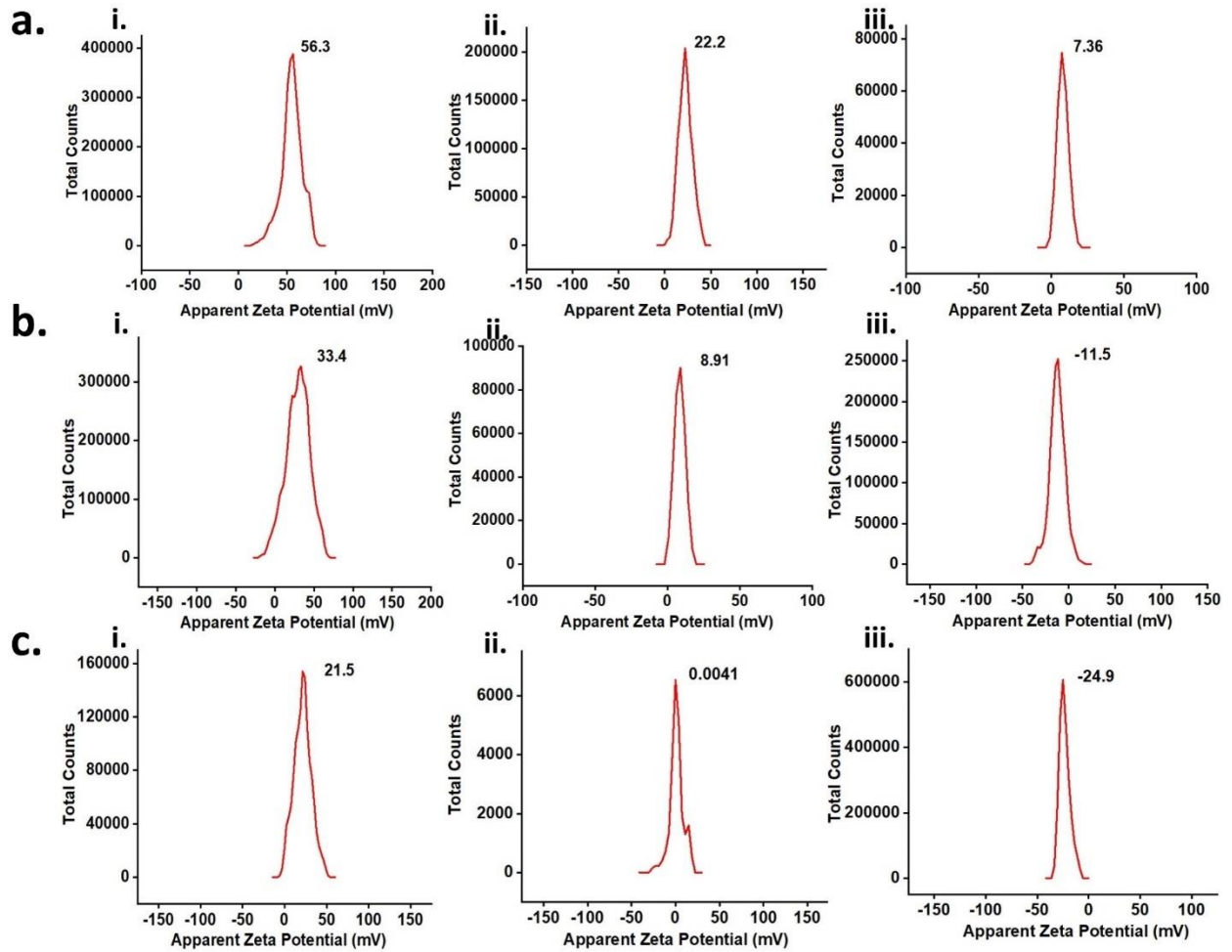
Fig 3. Showing the developed MSN ZETA potentials (a. i-iii) MCM-N at 5, 6.5, and 7.5 pH, respectively. (b. i-iii) MCM-Z at 5, 6.5, and 7.5 pH, respectively. (a. i-iii) MCM-ZD at 5, 6.5, and 7.5 pH, respectively. (d) ZETA potential values.

3.7 Release study analysis.

Studies have shown that charged nanochannels exhibit selective transport of molecules based on the surface charge and its interaction with the transported species.[51, 52] This work demonstrates this concept using positively charged CV+ molecules and negatively charged mesoporous silica MCM-Z. By loading CV+ onto MCM-Z at pH 8.5, we leverage the electrostatic interactions between the oppositely charged species; a change in pH around 7.5 triggers the release of the molecule. As illustrated in Fig 4.a and ii, the strong electrostatic interaction at pH 7.5 prevents significant release due to the tight binding between CV+ and the silica surface. At pH 5.0, a dramatic release of CV+ was triggered by electrostatic repulsion, as illustrated in Fig 4.a and ii. Notably, the release exhibited a marked dependence on pH, showcasing a highly quantitative response. However, a striking shift occurred at pH 5.0, significantly increasing CV+ release, MCM-Z (68%), and MCM-ZD (74%). These results highlight the pH-tuned delivery potential of these materials for applications like controlled molecule delivery. This pH-controlled release mechanism highlights the potential of charged nanochannels for controlled delivery applications.
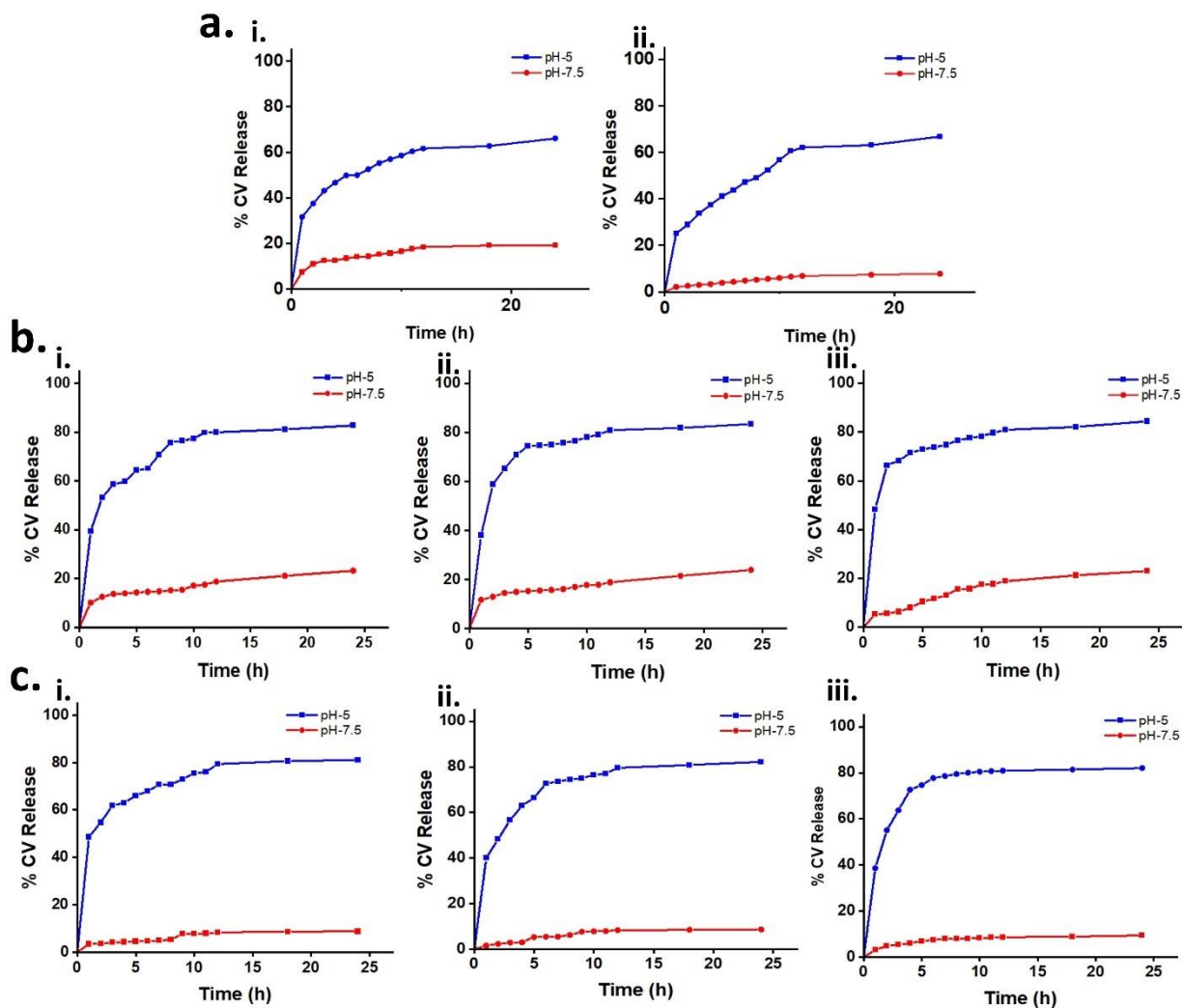
Fig 4. Showing the release study profile of CV+. (a) room temperature i. MCM-Z, and ii. MCM-ZD. (b) MCM-Z at various temperatures (i). 37°C (ii). 41°C, and (iii). 47°C respectively. (c) MCM-ZD at various temperatures (i). 37°C (ii). 41°C, and (iii). 47°C respectively.

We also established the pH-dependent release of a dye molecule (CV+) from two mesoporous silica materials, MCM-ZD and MCM-Z, at various temperatures (Fig 4. b&c. i-iii). At a neutral pH of 7.5, the minimal release occurred due to electrostatic solid attraction connecting the mesoporous silica and CV+ (Fig 4. b&c. i-iii). However, electrostatic repulsion triggered significant release under acidic conditions (pH 5.0), reaching 81-82% for MCM-ZD and 78-83%

for MCM-Z, regardless of temperature (37-47°C). These findings suggest that both materials exhibit promising pH-controlled release properties, with potential applications in drug delivery systems where targeted release at specific acidic tumor environments is desired.

The results of the desorption experiments suggest that temperature has little to no impact on the CV+ release from the nanochannels of MCM-ZD and MCM-Z. This is evident from the similar release percentages observed across different temperatures: 78% and 82% for MCM-Z and MCM-ZD at 37°C, 81% and 82% at 41°C, and 83% and 81% at 47°C, respectively (omitting in-text citations for brevity). This consistency implies that temperature within the tested range does not significantly influence the release mechanism.

4. Conclusion

This study reports mesoporous silica's successful synthesis and functionalization for controlled molecule delivery applications. The synthesized materials were thoroughly characterized. Crystal Violet dye was used as a model molecule to examine release activities at room temperature, controlled temperature, and various pH values. Notably, a significant difference in release was observed between pH 7.5 and 5 for MCM-ZD and MCM-Z nanoparticles. As expected, dextran-gated MCM-Z exhibited higher delivery at pH 5 more than MCM-ZD due to the pH-responsive nature of the incorporated molecules. Interestingly, the release profiles at room and controlled temperatures were comparable. This work presented a successfully functionalized MSN with succinic anhydride in 1,4-dioxane, achieving the desired level of surface charge for the first time. This new functionalization approach endows MSN with unique properties highly desirable for targeted delivery applications.

Acknowledgments

References

1. Mitchell, M.J., et al., *Engineering precision nanoparticles for drug delivery.* Nature reviews drug discovery, 2021. **20**(2): p. 101-124.
2. Liu, R., et al., *Advances of nanoparticles as drug delivery systems for disease diagnosis and treatment.* Chinese chemical letters, 2023. **34**(2): p. 107518.
3. Malik, S., K. Muhammad, and Y. Waheed, *Emerging applications of nanotechnology in healthcare and medicine.* Molecules, 2023. **28**(18): p. 6624.
4. Kumar, Y., et al., *Functionalized nanoparticles: Tailoring properties through surface energetics and coordination chemistry for advanced biomedical applications.* Nanoscale, 2023. **15**(13): p. 6075-6104.
5. Yanagisawa, T., et al., *The preparation of alkyltrimethylammonium–kanemite complexes and their conversion to microporous materials.* Bulletin of the chemical society of Japan, 1990. **63**(4): p. 988-992.
6. Xu, B., et al., *Multifunctional mesoporous silica nanoparticles for biomedical applications.* Signal Transduction and Targeted Therapy, 2023. **8**(1): p. 435.
7. Zhuang, J., Y. Yu, and R. Lu, *Mesoporous silica nanoparticles as carrier to overcome bacterial drug resistant barriers.* International Journal of Pharmaceutics, 2023. **631**: p. 122529.
8. Vallet-Regi, M., et al., *A new property of MCM-41: drug delivery system.* Chemistry of Materials, 2001. **13**(2): p. 308-311.
9. Santos, H., et al., *Mesoporous materials as controlled drug delivery formulations.* Journal of drug delivery science and technology, 2011. **21**(2): p. 139-155.
10. Zhang, J. and J.M. Rosenholm, *The viability of mesoporous silica nanoparticles for drug delivery.* Therapeutic delivery, 2015. **6**(8): p. 891-893.
11. Mamaeva, V., C. Sahlgren, and M. Lindén, *Mesoporous silica nanoparticles in medicine—Recent advances.* Advanced drug delivery reviews, 2013. **65**(5): p. 689-702.
12. Aznar, E., et al., *Gated materials for on-command release of guest molecules.* Chemical reviews, 2016. **116**(2): p. 561-718.

13.   Yang, P., S. Gai, and J. Lin, *Functionalized mesoporous silica materials for controlled drug delivery.* Chemical Society Reviews, 2012. **41**(9): p. 3679-3698.

14.   Wu, S.-H., C.-Y. Mou, and H.-P. Lin, *Synthesis of mesoporous silica nanoparticles.* Chemical Society Reviews, 2013. **42**(9): p. 3862-3875.

15.   Mal, N.K., M. Fujiwara, and Y. Tanaka, *Photocontrolled reversible release of guest molecules from coumarin-modified mesoporous silica.* Nature, 2003. **421**(6921): p. 350-353.

16.   Casasús, R., et al., *Toward the development of ionically controlled nanoscopic molecular gates.* Journal of the American Chemical Society, 2004. **126**(28): p. 8612-8613.

17.   Llopis-Lorente, A., et al., *Mesoporous silica materials for controlled delivery based on enzymes.* Journal of Materials Chemistry B, 2017. **5**(17): p. 3069-3083.

18.   Descalzo, A.B., et al., *The supramolecular chemistry of organic–inorganic hybrid materials.* Angewandte Chemie International Edition, 2006. **45**(36): p. 5924-5948.

19.   Slowing, I.I., et al., *Mesoporous silica nanoparticles as controlled release drug delivery and gene transfection carriers.* Advanced drug delivery reviews, 2008. **60**(11): p. 1278-1288.

20.   Trewyn, B.G., et al., *Mesoporous silica nanoparticle based controlled release, drug delivery, and biosensor systems.* Chemical communications, 2007(31): p. 3236-3245.

21.   Rosenholm, J.M., C. Sahlgren, and M. Lindén, *Towards multifunctional, targeted drug delivery systems using mesoporous silica nanoparticles–opportunities & challenges.* Nanoscale, 2010. **2**(10): p. 1870-1883.

22.   Rosenholm, M., *J., Sahlgren, C., Lindén, M., 2011. Multifunctional mesoporous silica nanoparticles for combined therapeutic, diagnostic and targeted action in cancer treatment.* Curr. Drug Targets. **12**: p. 1166-1186.

23.   Jafari, S., et al., *Mesoporous silica nanoparticles for therapeutic/diagnostic applications.* Biomedicine & Pharmacotherapy, 2019. **109**: p. 1100-1111.

24.   Fernandes, N.B., et al., *Multifunctional engineered mesoporous silica/inorganic material hybrid nanoparticles: Theranostic perspectives.* Coordination Chemistry Reviews, 2023. **478**: p. 214977.

25.   Pu, X., et al., *Mesoporous silica nanoparticles as a prospective and promising approach for drug delivery and biomedical applications.* Current cancer drug targets, 2019. **19**(4): p. 285-295.

26.   Castillo, R.R. and M. Vallet-Regí, *Functional mesoporous silica nanocomposites: biomedical applications and biosafety.* International Journal of Molecular Sciences, 2019. **20**(4): p. 929.

27.   Yin, P.T., et al., *Overcoming chemoresistance in cancer via combined microRNA therapeutics with anticancer drugs using multifunctional magnetic core–shell nanoparticles.* ACS applied materials & interfaces, 2018. **10**(32): p. 26954-26963.

28.   Zhang, L., et al., *Tailored synthesis of octopus-type janus nanoparticles for synergistic actively-targeted and chemo-photothermal therapy.* Angewandte Chemie International Edition, 2016. **55**(6): p. 2118-2121.

29.   Hu, J.-J., et al., *A positive feedback strategy for enhanced chemotherapy based on ROS-triggered self-accelerating drug release nanosystem.* Biomaterials, 2017. **128**: p. 136-146.

30.   Muñoz-Espín, D., et al., *A versatile drug delivery system targeting senescent cells. EMBO Mol Med. 2018; 10: e9355*.

31.   Sancenón, F., et al., *Gated silica mesoporous materials in sensing applications.* ChemistryOpen, 2015. **4**(4): p. 418-437.

32.   De Luis, B., et al., *Engineering chemical communication between micro/nanosystems.* Chemical Society Reviews, 2021. **50**(16): p. 8829-8856.

33.   de Luis, B., et al., *An interactive model of communication between abiotic nanodevices and microorganisms.* Angewandte Chemie International Edition, 2019. **58**(42): p. 14986-14990.

34.   de Luis, B., et al., *Nanoprogrammed Cross-Kingdom Communication Between Living Microorganisms.* Nano Letters, 2022. **22**(5): p. 1836-1844.

35. Croissant, J.G., et al., *Mesoporous silica and organosilica nanoparticles: physical chemistry, biosafety, delivery strategies, and biomedical applications.* Advanced healthcare materials, 2018. **7**(4): p. 1700831.

36. Park, S.S., M. Santha Moorthy, and C.-S. Ha, *Periodic mesoporous organosilicas for advanced applications.* NPG Asia Materials, 2014. **6**(4): p. e96-e96.

37. Gisbert-Garzaran, M., et al., *Designing mesoporous silica nanoparticles to overcome biological barriers by incorporating targeting and endosomal escape.* ACS applied materials & interfaces, 2021. **13**(8): p. 9656-9666.

38. Tapaswi, P.K., et al., *Fast, selective adsorption of Cu2+ from aqueous mixed metal ions solution using 1, 4, 7-triazacyclononane modified SBA-15 silica adsorbent (SBA-TACN).* Journal of Solid State Chemistry, 2014. **211**: p. 191-199.

39. Moorthy, M.S., et al., *Red fluorescent hybrid mesoporous organosilicas for simultaneous cell imaging and anticancer drug delivery.* RSC Advances, 2014. **4**(82): p. 43342-43345.

40. Zhang, X., J. Lanter, and Z. Sui, *Expert Opin.* Ther. Patents., 2009(19): p. 1239.

41. Moorthy, M.S., et al., *Multifunctional periodic mesoporous organosilicas for biomolecule recognition, biomedical applications in cancer therapy, and metal adsorption.* European Journal of Inorganic Chemistry, 2013. **2013**(17): p. 3028-3038.

42. Li, Z., N. Song, and Y.-W. Yang, *Stimuli-responsive drug-delivery systems based on supramolecular nanovalves.* Matter, 2019. **1**(2): p. 345-368.

43. Hershberger, K.K., A.J. Gauger, and L.M. Bronstein, *Utilizing stimuli responsive linkages to engineer and enhance polymer nanoparticle-based drug delivery platforms.* ACS Applied Bio Materials, 2021. **4**(6): p. 4720-4736.

44. Park, C., et al., *Enzyme responsive nanocontainers with cyclodextrin gatekeepers and synergistic effects in release of guests.* Journal of the American Chemical Society, 2009. **131**(46): p. 16614-16615.

45. Hu, C., et al., *Tannin as a gatekeeper of pH-responsive mesoporous silica nanoparticles for drug delivery.* RSC advances, 2015. **5**(104): p. 85436-85441.

46. Gerion, D., et al., *Paramagnetic silica-coated nanocrystals as an advanced MRI contrast agent.* The Journal of Physical Chemistry C, 2007. **111**(34): p. 12542-12551.

47. Huh, S., et al., *Organic functionalization and morphology control of mesoporous silicas via a co-condensation synthesis method.* Chemistry of materials, 2003. **15**(22): p. 4247-4256.

48. Sonu, K., *Design strategies for charge reversal and temporally regulated functionalities in porous and non-porous systems*. 2019, Jawaharlal Nehru Centre for Advanced Scientific Research.

49. Dias, D.R., A.F. Moreira, and I.J. Correia, *The effect of the shape of gold core–mesoporous silica shell nanoparticles on the cellular behavior and tumor spheroid penetration.* Journal of Materials Chemistry B, 2016. **4**(47): p. 7630-7640.

50. Dai, L., et al., *Redox-responsive nanocarrier based on heparin end-capped mesoporous silica nanoparticles for targeted tumor therapy in vitro and in vivo.* Langmuir, 2014. **30**(26): p. 7867-7877.

51. Manzo, V., et al., *Determination of crystal violet in water by direct solid phase spectrophotometry after rotating disk sorptive extraction.* Talanta, 2013. **106**: p. 305-308.

52. Sparreboom, W., A. van den Berg, and J.C. Eijkel, *Principles and applications of nanofluidic transport.* Nature nanotechnology, 2009. **4**(11): p. 713-720.